flexLiTE: flexible micro-LED integrated optoelectrodes for minimally-invasive chronic deep-brain study

Eunah Ko[1], Mihály Vöröslakos[1, 2], György Buzsáki[2*], Euisik Yoon[1, 3, 4*]

[1] Department of Electrical Engineering and Computer Science, University of Michigan, Ann Arbor, MI 48109, USA
[2] Neuroscience Institute, Langone Medical Center, New York University, New York, NY 10016, USA
[3] Department of Biomedical Engineering, University of Michigan, Ann Arbor, MI 48109,
[4] Center for Nanomedicine, Institute for Basic Science (IBS) and Graduate Program of Nano Biomedical Engineering (Nano BME), Advanced Science Institute, Yonsei University, Seoul 03722, South Korea
Correspondence: Euisik Yoon (esyoon@umich.edu)

Abstract

Understanding complex neuronal circuitry and its functions of a living organism requires a specialized tool which is capable of (i) recording a large ensemble of neuronal signals at single cell resolution, (ii) modulating neuronal activities optogenetically at the same time, and (iii) sustaining functionality for long-term chronic experiments without significant tissue degeneration or device migration. We hereby present an ultra-flexible, minimally-invasive, Michigan-type neural probe for chronic opto-electrophysiology studies: flexLiTE (flexible micro-LED integrated optoelectrodes). flexLiTE incorporates monolithically integrated, soma-sized micro-inorganic LEDs (μILEDs, 12 individually operated) and 32 recording electrodes. The stimulation and recording modalities are integrated by stacking two modules on a flexible shank, resulting in a 115 μm-wide,12 μm-thick, 10 mm-long optoelectrode. From prototype devices, we demonstrated the reliable operation of flexLiTEs for recording and modulation of hippocampal neurons in a freely moving mouse for over ~2 month.

Introduction

Recent advances in micro-fabricated deep-brain implantable neural interfaces unraveled the circuit connectivity of neurons to give a hint of mechanisms behind neurological disorders that may lead to the treatment [1-4]. Yet, long-term (weeks to months) recording along with optogenetic stimulation remains as a key challenge in implantable probes for deep-brain regions. The penetration volume and the mechanical stiffness should be reduced to prevent the insertion damage, foreign-body induced tissue reaction and following fibrotic scarring from micro motions, which degrades quality of signals and control of cells over time [4-6].

Flexible substrates can alleviate the mechanical stiffness and tissue damage compared to rigid, silicon probes [7-8]. Flexible probe can be made in a relatively thin substrate. The stiffness of a probe shank can be defined as $Ewt^3/4L^3$, where E is the Young's modulus of the shank material, w is the width of the shank, t is the thickness, and L is the total length. Taking advantage of <10 GPa of Young's modulus and reduced thickness, flexible polymer-based neural probes are beneficial for less tissue reaction and minimally-

invasiveness for long-term chronic recording [9-10].

Among many flexible substrate polymer materials such as parylene-C, SU-8, and polyimide)[11-14], recent studies showed that polyimide (PI) has excellent microfabrication and bio compatibility [15-20]. It can withstand thermal processes lower than its glass transition temperature of 360 °C [21], and can be easily micro-patterned using dry reactive ion etching (RIE). Recent progress showed that the recording electrodes on a polyimide substrate can be integrated in a small area for high density, aiming to record spikes in a large-population of cells [22-23].

Even though the stability of the polyimide-based flexible neural probes has been studied extensively, not much progress has been done for integration of perturbation sources. Among many neuromodulation methods, optogenetics is one of the most widely used ones by virtue of its high spatiotemporal controllability. The genetically modified opsins that are present on the surface of the cell membrane are activated by light at a specific wavelength, leading to neuronal spiking or inhibition [24-28]. The requirements for optogenetic light source that may suit for minimally-invasive flexible neural interface would be as follows: (i) light shall illuminate and perturb only a small group of cells with high spatiotemporal resolution; (ii) footprint should be small enough to fit the volume that is similar to the state-of-the-art flexible recording probes (~100 μm wide, ~10 μm thick]; and (iii) each light source should be controlled individually and confined only onto the target region of the brain without leaking light to non-targeted areas.

Micro-sized inorganic light-emitting-diodes (μILED) was first monolithically integrated onto a silicon shank [29]. Wu et al. demonstrated the scalable, individually operated, soma-sized (10x15 μm) μILED optoelectrode in a typical Michigan type probe configuration [29]. Compared to recent light delivery schemes, such as optical fibers, multi-photon stimulation, or waveguide technologies [30-34], this μILED optoelectrode has many advantages including high scalability, fabrication process compatibility (mass-production by utilizing wafer-level manufacturing), and high temporal resolution inside the deep-brain region [35-39].

In this work we present a ultra-flexible Michigan type optoelectrode by monolithically integrating cell-sized μILEDs into a polyimide substrate. This approach is different from previous ones because we fabricated the probes through wafer-level processing instead of die transfer of each individual μILEDs manually. The first prototype optoelectrodes incorporate12 μILEDs onto 115 μm-wide, 6 μm-thick and 10 mm-long polyimide probe shank. With the μILEDs that span 1 mm at the tip side of the probe, flexLiTE can induce optogenetic stimulation while recording single neuron activities from 32 recording sites precisely located in proximity of μILEDs. This 32-channel flexible recording electrodes (area of 195 μm^2) were separately fabricated and assembled with the μILEDs module. An interposer was used for assembly from ball bonding of the stacked modules. We demonstrated the long-term chronic in-vivo optogenetic experiments of flexLiTEs in a freely moving mouse.

Results

Modularity of flexLiTE optoelectrodes

The flexLiTE explores the feasibility of a polyimide-based flexible optoelectrode integrated with micron-sized ILEDs for chronic optogenetic stimulation and recording with ultra-flexibility (Fig. 1A). Two modules (a blue-light illuminating stimulation module and a recording module) are integrated into one system through stacking (Fig. 1B and C). The flexLiTE is highly flexible since it is made of polyimide materials that passivates all the components in a total thickness of 12 μm (Fig. 1D and E). The device is composed of multiple individual parts: (i) the blue-ILEDs integrated on a flexible polyimide substrate for optogenetic stimulation, (ii) the recording electrodes on a flexible polyimide substrate for recording wide-band neuronal signals, both spikes and local field potentials (LFPs), (iii) the interposer for stacking and aligning two modules ((i) and (ii)), (iv) the custom-made cable that connects the interposer and a headstage, and (v) the headstage PCB with an Omnetics connector. All the components are assembled into a complete flexible optoelectrode system (Fig. 1F). The LED/recording modudes are separately characterized before assembly. The 12 μILEDs can all be individually controlled, either activated at the same time (Fig. 1G) or individually (Fig. 1H).

There are several vital reasons behind this modular approach. First, this allows for function-based unit device manufacturing, which increases fabrication yield. The overall yield of an electronic system is significantly affected by a number of added layers of fabrication. As an additional mask step increases, the wafer fabrication yield is lowered [40-41]. This is even more aggregated when a polyimide layer fabrication step is added. Controlling the thickness of polymer layers is not as good as other solid materials such as metal, oxide, or semiconductor due to the nature of spin coating of polymers. Second, the modular approach is flexible in enabling a specific function of choice. For example, we can use only the stimulation function or only the recording function. Even other type of functions can be added such as temperature sensing, chemical sensing, fluidic drug delivery, etc. This also allows for reduced manufacturing time from less mask steps incorporated. In this work, we integrated two modules for stimulation and recording functions through an interposer.

Design and fabrication of µILED probe modules

The µILED integrated flexible stimulation probe module (abbreviated as 'LED probe', noted as 'LED' in Fig. 2 and Fig. 3) consists of total 12 micron-sized (6 µm × 15 µm × 2.5 µm) Gallium Nitride (GaN) ILEDs. They span ~1 mm long top-down from the tip of the shank, each LED individually controlled to stimulate neurons at cellular resolution [29].

LEDs are composed of GaN quantum wells that emit blue light with λpeak ≈ 467 nm. 12 LEDs are integrated on a 6 µm thick polyimide substrate and are connected to the backend through metal traces. The LED probe has total 10 mm long and electrically connected to the headstage PCB through an interposer (ball bonded) and a custom-made flexible cable (20 mm long).

The fabrication processes of the LED probe started with a GaN-based multi-quantum-well (MQW) grown on Silicon (111) wafer (4-inch, Fig. 2A:1-9). Mesa structures of LEDs were defined by two steps: one for the first mesa etching down to the n-contact region of the LED (~ 500 nm), and second for isolating the mesa by etching down to the field silicon region (~ 2 µm, a total mesa stack height of ~ 2.5 µm). The silicon region was exposed for the full-coverage of LEDs by polyimide in the later process. A mixture gas of Cl2 and BCl3 was used for RIE definition of the mesa.

The wafer was then passivated with an oxide thin layer (~ 500 nm) for protecting the mesa (Fig. 2A:2-3). The p-GaN metal contact is defined using SPR 220 3.0 photoresist lithography. Ni/Au (total 10 nm thick) metal stacks were defined and annealed at 500 °C by rapid thermal annealing (RTA) for lowering contact resistance of the metal contact [29].

The contact holes for n-GaN were opened and wafer was passivated with Al_2O_3. On top the polyimide 2610 (HD Microsystems, Parlin, NJ, United States) was spun and cured at 350 °C inside the oven using H2/N2 environment (thickness ~ 1.5 µm after cure). The contact holes were etched and the n-GaN contact metal was defined along with providing p-GaN traces using the double-layer photoresist lithography. This double-layered undercut structure is much beneficial for lift-off. Cr and Au layers (total 300 nm) were sputtered (Lab 18-01, Kurt J. Lesker Company, PA, US) and lifted-off. Finally, the LED p-GaN contact metal/intermediate metal and n-GaN contact metal were connected to the backend ball bonding pads through 300 nm-thick metal traces of gold.

Next the second polyimide layer was spun and cured (~ 2.5 µm). The surface of the first polyimide layer was treated with oxygen plasma for better adhesion between PI-to-PI (Fig. 2A:4-5). Then the bonding pads at the backend of the LED probe were opened, and the sacrificial layer (Chromium, total 225 nm) was sputtered (Lab 18-01) on the whole wafer. The wafer was transferred to a carrier wafer for complete removal of a silicon substrate with an adhesive film. The backside silicon was removed by deep-reactive-ion-etching (DRIE) (Fig. 2A:6). After she silicon was completely removed, the field oxide was etched away in a buffered HF solution. The exposed bottom surface of the n-GaN of LED mesa was covered by Titanium and Aluminum (200 nm).

Finally, the third polyimide layer was spun and cured, surrounding the LEDs and traces all around with the flexible polyimide substrate (~ 2 µm thick, ~ 6 µm of total LED probe thickness, Fig. 2A:7-9). The through-holes for the ball bonding pads were opened and at the same time probe outline was defined. Then the wafer was put inside a Chromium etchant for probe release.

Design and fabrication of REC probe modules

The second module of flexLiTEs is the recording electrode probe ('REC probe'), which is composed of 32 electrodes. The electrodes are arranged in two rows that will be aligned with LEDs of the simulation probe module (or 'LED probe') on a 115 µm-wide, 6 µm-thick flexible

polyimide substrate (Fig. 2B and C). Total 32 traces were defined with 1 μm metal width and 1 μm space. The LED windows were opened with a 3.5 μm alignment margin from the edge of the LED (Fig. 2D). Fig. 3A shows the fabricated LED probe and REC probe (left and right, respectively) and the enlarged image of the single LED illuminating through a window opening. The probe-to-probe stacking margin was given in Fig. 3D with the dimensions used for the probe design in Fig. 3B and C. The REC probe is to be placed on top of the LED probe to expose the recording electrodes closely to the cells. The area of the recording electrode was 195 μm^2. The vertical and lateral distances of the electrodes were 17 and 22 μm, respectively, while the vertical distance between two electrodes in the same column was 64 μm, giving ~ 1000 μm of covering span from top to bottom. The fabrication process flow is summarized and represented in Fig. 2B:1-7 (the side cross section view) and Fig. 2C:1-5 (top-view).

The fabrication of REC probes started with a silicon wafer with a thin oxide grown on top (Fig. 2B:1-2 and C:1). First, the Chromium sacrificial layer (~ 225 nm) was defined first. Then the first polyimide layer was spun and cured (~ 2 μm), followed by the bottom shield metal definition which works for shielding the electromagnetic interference (EMI) generated from the LED probe. The shielding layer was composed of Titanium and Gold (~ 300 nm) and was ball bonded to the ground at the end of the assembly process (Fig. 2C:1, the top view of defined shield with the LED window patterned).

On the top of the bottom-shield layer, the second polyimide layer was spun and cured (~ 1.8 μm thick) as the intermediate layer between the first metal (the shield) and the second metal (the traces for connecting recording electrodes and the backend ball bonding pads) (Fig. 2B:3-4 and C:2-3). The Al2O3 layer was deposited to passivate the traces (30 nm thick) [42-43]. Next, Titanium and Gold metal composites were defined for metal traces by lift-off. The top side of the traces were covered with an additional passivation layer (~ 15 nm) and the oxide is patterned, leaving the probe-outline boundary free from any oxide covering. Next, the third polyimide layer was spun and cured (~ 2 μm thick), followed by recording electrode formation.

The recording electrode surface was roughened to lower the impedance (Fig. 2B:5-7 and C:4-5) [22]. Finally, the REC probe outline was defined by RIE, and devices were released in the Chromium etchant.

Assembly of flexLiTE optoelectrodes

We introduced a thin silicon-based interposer structure as an intermediate assembly part to integrate the two modules: LED probe and REC probe. The interposer is composed of an array of bonding pads in the front-end for connecting the probe modules, and another array of bonding pads in the back-end for connecting the cable to the headstage PCB. Fabrication starts with a 200 μm-thick silicon wafer. A 500 nm-thick oxide layer was first deposited using plasma enhanced chemical vapor deposition (P5000 PECVD, Applied Materials Inc., CA, US). Then, metal pads and traces were evaporated and lifted off, leaving the bonding pads and the traces. Top of the metal traces was passivated by oxide and the bonding pad openings were made. The wafer was diced into individual small (6 mm × 6 mm) interposers and cleaned (Fig. 1F(ii)). Another assembly component is the cable (Fig. 1F(iii)). The fabrication is similar to the REC probe.

As a last step, the LED and REC probes were stacked first with coarse alignment (the REC probe goes on top of the LED probe) after treated with IPA. The stacked probe shank part was dipped into the DI water for fine alignment (self-aligned from surface tension; details explained in the method section) (Fig. 3E and F). The backend of the stacked probes was ball-bonded to the interposer and then passivated. Next, the cable was ball bonded to the interposer and the headstage PCB. Finally the connectors were attached to the PCB, and

the assembled flexLiTE optoeletrodes are ready for characterization and in-vivo experiments.

In vitro characterization of flexLiTE optoelectrodes

In pursuance of reliable in-vivo chronic experiments, full characterization of the assembled and ready-to-use flexLiTEs should be conducted thoroughly. Figure 4 represents the characterized results of three assembled flexLiTEs. The characterization methods are summarized in the Method section. We tested the total 36 LEDs and 96 recording electrodes, among which 1 LED and 5 recording electrodes were not-functioning. The results represent the characteristics from 35 LEDs and 91 recording electrodes. The features of the flexLiTEs include: current-voltage (I-V) characteristics of LEDs, light power (radiant flux, Φ_e) versus current, light wavelength spectrum at various current levels, impedance of the recording electrodes, and heating effect of the LEDs from COMSOL Multiphysics simulation.

Figure 4A shows the I-V characteristics of all LEDs measured from 0 V to 7 V under a current compliance of 100 μA. The dashed-purple lines show the maximum and minimum I-V curves from all measured results (criteria for the max/min is the voltage value at 100 μA). Compared to the LEDs formed on asilicon shank that was published in 2015 [29], the I-V shows higher parasitic resistance due to the polyimide incorporated in the fabrication processes. The oxygen plasma RIE of polyimide could leave a thin residue layer on top of the metal contact holes, leading to a degradation of the contact resistance [47]. The solution can be a Fluorine gas added for etching the contact holes; however, this needs to be investigated thoroughly as future work.

Figure 4B shows the percentage of the current value at 3.8 V of input voltage (Vin) for the range from 10 μA to 16 μA. Note that about ~ 80 % of the LEDs have current value between 11 μA ~ 15 μA (note that the Vin used during in-vivo testing was 3.8 V). The wavelength spectrum of blue-light generated from the LEDs were tested for various current levels (Fig. 4C). The inset of Fig. 4C shows the magnified view of the wave spectrum at a current level of 5 μA (and to compare the inset with the others, numbers are denoted for the arbitrary unit (a. u.) amplitude (y) axis). The peak amplitude was measured to be ranging at 466-468 nm (467 nm at 15 μA of testing current).

Figure 4D shows the radiant flux (Φ_e) measured for 15 and 50 μA of current levels. The median values points were ~ 1.5 and ~ 4.5 μW for 15 and 50 μA, respectively. Considering the lower threshold value (optical power needed) of 1 mW/mm^2 for activating opsins, the optical power measured from flexLiTE optoelectrodes is suitable for optogenetic stimulation [44-46]. Following the electrical and optical characterization, we tested the impedance of the recording electrodes in-vitro. (see the Methods section for the testing settings.)

Figure 4E denotes the distribution of impedance measured from the recording electrodes using the Intan system. More than 90 % of the electrodes showed the impedance value between 1 ~ 1.5 MΩ, which is suitable to be used for recording neural activities inside the target region of the brain. The impedance value was then further tracked during the in-vivo experiments, which will be described in in-vivo validation section. As the last part of characterization, the heating effect was evaluated by COMSOL Multiphysics simulations. The 6 μm × 15 μm area (LED size, Fig. 3B) was designated as the light power generating

area (blue colored region in Fig. 4G, left). Thermal conductivity of 0.12 W/m·K was used for polymide substrate and compared with the result from the silicon shank one (with the same dimension, total thickness of 12 μm) which has a much higher thermal conductivity of 148 W/m·K. The probing point of the temperature was set to be at 8 μm away from the LED top surface in z-axis direction, as this would be where the neurons might be presumable located from our previous in-vivo experiments. The input power was applied for a 1 sec long in a square function with a 10 % duty cycle (which is actually the case for our in-vivo experiments).

Figure 4F shows the corresponding temperature of the probing point during 5 cycles of various input power from 37 μW to 105 μW. These values were chosen from the actual power at the input voltage range of 3.0 V to 4.5 V. For the comparison of the polyimide vs. silicon substrate, we used the input power of 60 μW (Vin = 3.8 V, I = 16 μA) (Fig. 4G, right, total 20 cycles). Figures 4F and G both show that even with the continuous cycles of input power, the peak temperature value does not change and as soon as the input pulse becomes off, the temperature rapidly goes down to the baseline temperature (which is 310.15 K = 37 °C). Even with input power of 105 μW, the difference between the temperature peak and the baseline is < 1 °C, which secures that temperature increase of the brain is negligible for in-vivo studies. The black-colored curve shown in Fig. 4G represents the temperature variation of the silicon substrate μLED probe, and it can be confirmed that the temperature increase is much less than that of polyimide-based optoelectrodes. However, simulation result verified that flexLiTE optoelectrode also is suitable.

In-vivo validation of flexLiTE optoelectrodes in a freely moving mouse

A fully assembled flexLiTE optoelectrode (12 μLEDs and 32 recording electrodes) was implanted in a transgenic mouse expressing ChR2 selectively in CamKII expressing excitatory cells. flexLiTE was inserted into the dorsal hippocampus using a glass pipette as mechanical shuttle (the probe tip was attached to the glass pipette using polyethylene glycol, Fig. 5A and B). Impedance of recording electrodes was tested before the implant (Fig. 5C). After reaching the target depth (1.2 mm from the surface of the brain) the glass pipette was retracted, leaving the flexLiTE probe inside the brain. Opto-electrophysiology recordings started 2 weeks after the surgery to let the tissue heal around the probe tip.

Spontaneous neuronal activity was recorded (n = 3 sessions) and 7 putative single units were isolated (4 putative pyramidal and 3 putative interneurons Fig. 5D and E). The details of cell classification criteria can be found in the Method section. Illumination of the third LED from the tip of the probe (Vin amplitude of 3.8 V, 1 sec long pulse with 10 % duty cycle, 500 trials, Fig. 5G) elicited spiking in 4/4 (100%) putative pyramidal and in 1/3 (33%) putative interneurons (Fig. 5G and H). The light-induced response of an example cell is shown in Fig. 5D (mean firing rate is 1.45 Hz without and 28.47 Hz with stimulation, $p < 0.05$; Wilcoxon signed rank test).

Light-induced neuronal activity was recorded at day 18 and day 26, and the same LED (third from the tip, Fig. 6A) was used for stimulation (Vin amplitude of 3.8 V, 1 sec long pulse with 10 % duty cycle). The putative pyramidal cells were strongly influenced by the blue-LED illuminated 467 nm of wavelength of light (mean firing rate is 1.45 and 0.93 Hz without and 28.47 and 25.49 Hz with stimulation, on day 18 and 26, respectively, $p < 0.05$; Wilcoxon

signed rank test) confirming that the flexLiTE functioned as stimulation/recording optoelectrode for ~ 4 weeks (Fig. 6B and C). To determine the in-vivo functionality of the recording electrodes, the impedance was measured at 1kHz during each recording sessions (Fig. 6D and E, note that 3 recording electrodes had higher than 5 MΩ impedance since the first recording session). According to the impedance data the electrode did not lose its recording functionality throughout our experiment.

Discussion

The flexLiTE optoelectrode was demonstrated for the first time for chronically modulating and recording the brain neuronal circuitry through chronic in-vivo experiments for > 1 month of duration subsequent to the surgery of the probe. The modular structure of flexLiTE can expedite the neuroscience study in terms of both efficiency in surgery and device and assembly yields. The unit function probes ('LED probe' and 'REC probe') can be fabricated separately and assembled via an interposer. This enhance the yield of probes and provide fast turn-around time because each module can be selectively assembled depending on the end users' need, simplifying manufacturing processes and fursnighing versatility. This modular reconfigurable approach allows the probe backend to be elongated into any length (in this work the length of the cable was 20 mm but it can be elongated at any preferred length) to meet the need that the neuroscience experiment requires. The main design for the prototype probe was to cover a 1 mm span for a target region of brain with LEDs and recording electrodes, each 12 and 32 respectively, on a ultra-flexible polyimide substrate for long-term chronic experiments. These device elements were incorporated into a polyimide substrate with a dimension of total 10 mm long (only the shank region), 115 μm of shank width, and 12 μm of shank thickness. By virtue of matched surface energy of polyimide we could realize multi-module-stacked structures where the REC probe was placed on top of the LED probe with precise alignment from surface tension when placed and dried up in an aqueous solution such as IPA. The characteristics of the LEDs and recording electrodes, including the thermal simulation result of the brain tissue heating due to LED driving, showed the flexLiTE optoelectrode is suitable for in-vivo experiments. FlexLiTE optoelectrodes were implanted in the CA1 region of the hippocampus of the mouse. Once the tissue was healed after two weeks of implantation, chronic in-vivo experiments were conducted to validate the capacity of the flexLiTE as a fully functional chronic optoelectrode. First, the REC probe was proven through cell classification of putative pyramidal cells and interneurons. Secondly, the optogenetic neuromodulation was validated by recording of μILED illumination-induced spikes at 467 nm in wavelength (blue light). Compared with non-illuminating states we revealed the stimulation-induced spiking rates increased significantly. Lastly, the chronic-capability was validated by conducting the same in-vivo experiments over time. The spiking rate discrepancy between non-/ and illuminating states in the 4th week after implant showed the similar results to that of the 2nd week. Recently, another chronic experiments showed the longevity of flexLiTE optoelectrodes for > 12 weeks, which can be further improved for several months. Our modular architecture of assembly is easily scalable to increase the density of μILEDs and recording electrodes by design variation, making flexLiTE optoelectrodes suitable for large-area chronic monitoring of neural circuits and targeted neuromodulation in long-term

behavioral studies.

Methods

flexLiTE fabrication and packaging

The LED probes, REC probes, interposers and cables were fabricated in the Lurie Nanofabrication Facility at the University of Michigan, Ann Arbor, Michigan. GaN-on-silicon wafers were purchased from Enkris (Enkris Semiconductor Inc., Suzhou, China). Polyimide 2610 and 2611 were spun and cured by the Laurell Spinner (Model Ws-650-23B, PA, United States) and Vacuum Oven (YES PB8-2B-CP, Yield Engineering Systems, CA, United States), respectively. The LED and REC probe traces were passivated for longevity enhancement by coating of Al_2O_3 (Oxford OpAL ALD). At the end of the front-side fabrication the wafer was coated with a PI adhesive and bonded to a carrier wafer by a wafer bonder (EVG 510, EV group, Sankt Florian am Inn, Austria). Two-step probe outline definition incorporates a mid-temperature curing for 1 hour, patterning through plasma RIE (Plasmatherm 790, Plasma-Therm, LLC, FL, United States), and high-temperature curing for 1 hour before released in a Cr etchant (Chromium Etch 1020, Transene Company, Inc., MA, United States). Polyimide-to-polyimide interfaces were surface treated with oxygen plasma (Tergeo Plasma cleaner, PIE Scientific LLC, CA, United States). Interposers were fabricated using a 200 μm thick silicon wafer and diced into 6 mm × 6 mm squares before assembly. All the lithography for the LED/REC probes was done using a stepper (GCA AS200 AutoStep) and the interposers and cables were patterned by a contact aligner (MA/BA-6 Mask/Bond Aligner).

Assembly processes except for the PCB fabrication (PCBWay, Shenzhen, China) was done in-house (EECS building, University of Michigan,Ann Arbor, MI, United States). Before the assembly, individually manufactured LED/REC probes were first surface treated with IPA (Isopropyl alcohol) making surfaces hydrophilic, and two probes are stacked (REC probe on top of the LED probe) for coarse alignment. Next, the probe shanks of the stacked probes were dipped and pulled out slowly from the DI water container where fine adjustment of alignment took place. Next, the stacked probes were ball bonded (K&S 4524-D, Kulicke and Soffa Industries, Inc., PA, USA) to the interposer using aluminum bumps. The 8 μm-thick, 20mm-long custom-made polyimide (PI2611) cables connected from the interposer to the headstage PCB by ball bonding. The 36-pin and 18-pin connectors (Omnetics Connector Corporation, MN, Unites States) were soldered to the PCB. Electrical connections of the fully assembled device were passivated by Epoxy (EPO-TEK 353ND-T, Epoxy Technologies, MA, USA).

Electrical and optical characterization

After flexLiTE probes were assembled, we characterized the current vs. voltage (I-V) and radiant flux vs. current (Φ_e-I) for LEDs and the impedance measurement of the recording electrodes (Ω-channel #). Total 3 probes were used for bench-top characterization. The I-V characteristic were measured using the source-meter (Keithly 2400, OH, US) and the Φ_e-I was measured using an optical power meter composed of the integrating sphere and spectrometer (FOIS-1, and Flame, Ocean Optics, FL, US). The entire

probe (10 mm long probe shank part) was placed under an integrating sphere. The size of the interposer was small enough to put the flexible probe inside the sphere to ensure the light from the LEDs are delivered to the optical measuring system. Optical power integration range was set to 400 – 500 nm in wavelength, where the maximum power measured was at 467 nm of wavelength. The Ω-channel # was measured at 1 kHz by Intan system (Intan RHD 32-channel recording headstage and RHD2000 USB interface board, Intan Technologies, CA, US). The probe shank was placed in a 1× phosphate buffered saline solution (MP Biomedicals, OH, US) and the impedance was measured for all 32 channels. Once the impedance was measured the probes were cleaned using IPA and DI water.

Thermal simulation

The flexLiTE LED design and configuration was taken into the COMSOL Multiphysics simulation for the thermal simulation. The same dimension of the device fabrication mask layout was used. The temperature measurement was estimated in the tissue 8 μm above the LED surface. (Note that the thickness of the REC probe is ~ 6 μm, and the second PI layer for the LED probe is ~ 2.5 μm.) The probe shank was presumed to be surrounded by the brain tissue. The actual electrical power was applied as input power for the simulation from a voltage range of 3.0 V to 4.5 V. For simplicity of thermal modeling, the materials that the LED probes are composed of for electrical isolation is only polyimide. The bio-heat transfer equations were used from [Pennes, J. Appl. Physiol. 1948 [51]]. All the related parameters were taken from [Wu et al., Neuron 2015 [29]] except for polyimide. We used the COMSOL material polyimide with a thermal conductivity of 0.12 W/m·K.

Animal experiments: In-vivo opto-electrophysiology

All experiments were approved by the Institutional Animal Care and Use Committee at New York University Medical Center. Animals were handled daily and accommodated to the experimenter before the surgery and homecage recordings. An adult male mouse (CaMKII-ChR2, 31 g) was kept in a vivarium on a 12-hour light/dark cycle and was housed two per cage before surgery and individually after it. Atropine (0.05 mg kg–1, s.c.) was administered after isoflurane anesthesia induction to reduce saliva production. The body temperature was monitored and kept constant at 36–37 °C with a DC temperature controller (TCAT-LV; Physitemp, Clifton, NJ, USA). Stages of anesthesia were maintained by confirming the lack of a nociceptive reflex. The skin of the head was shaved, and the surface of the skull was cleaned by hydrogen peroxide (2%). A custom 3D-printed base plate (Form2 printer, FormLabs, Sommerville, MA) [52] was attached to the skull using C&B Metabond dental cement (Parkell, Edgewood, NY). A stainless-steel ground screw was placed above the cerebellum and sealed with dental cement (Unifast LC, GC America). The location of the craniotomy was marked (2 mm posterior to Bregma and 1.5 mm lateral to midline) and a 700-μm craniotomy was drilled. After the dura was removed the flexiLiTE optoelectrode was inserted into the brain (1.2 mm depth from the surface of the brain) using a glass pipette with a tip diameter of 15-20 μm (3-000-203-G/X, Drummond Scientific, PA). The glass pipette was retracted, and the craniotomy was sealed with dura-gel (Cambridge Neurotech) and then covered with dental cement. Finally, a protective cap was built using copper mesh [52]. The mouse recovered for at least 7 days after surgery. Animal was recorded in its

homecage. The collected data was digitized at 20 kS/s using an RHD2000 recording system (Intan technologies, Los Angeles, CA).

Animal experiments: Controlling flexible μLEDs

Current-controlled stimulation was used to drive individual μLEDs (OSC1Lite [37]), 12-ch current source (https://github.com/YoonGroupUmich/osc1lite). The stimulation amplitude and waveform were defined using OSC1Lite's open-source graphical user interface.

Animal experiments: Single unit analysis

A concatenated signal file was prepared by merging all recordings from a single day. To improve the efficacy of spike sorting, stimulation induced onset and offset artefacts were removed before automatic spike sorting (50 ms before and 100 ms after the detected artefacts, linear interpolation between timestamps). Putative single units were first sorted using Kilosort [53] and then manually curated using Phy (https://phy-contrib.readthedocs.io/). After extracting timestamps of each putative single unit activity, peristimulus time histograms and firing rate gains were analyzed using a custom MATLAB (Mathworks, Natick, MA) script. To measure the effect of light on spiking, peristimulus time histograms (PSTHs) were built around stimulus onset (spike trains were binned into 10-ms bins). Baseline and light-induced spiking rate were calculated for each single unit. Baseline was defined as light-free epochs (700 ms) between trials and stimulation period as μLED was on (100 ms). Wilcoxon-signed rank test was used to compare the mean firing rate per trial during baseline and μLED stimulation [30-31].

Animal experiments: Cell-type classification

Recorded cells are classified into three putative cell types: narrow interneurons, wide interneurons, and pyramidal cells. Interneurons are selected by 2 separate criteria; narrow interneuron is assigned if the waveform trough-to-peak latency is less than 0.425 ms. Wide interneuron is assigned if the waveform trough-to-peak latency is more than 0.425 ms and the rise time of the autocorrelation histogram is more than 6 ms. The remaining cells are assigned as pyramidal cells. Autocorrelation histograms are fitted with a triple exponential equation to supplement the classical, waveform feature based single unit classification (https://cellexplorer.org/pipeline/cell-type-classification/) [54]. Bursts were defined as groups of spikes with interspike intervals < 9 ms.

Animal experiments: In-vivo impedance measurement

The impedance of the recording probe was measured during each recording session (n=5 sessions, Fig. 6) using an RHD USB interface board (Intan Technologies LLC, CA, USA). The impedance test measurements were performed at 1 kHz frequency. This measurement provides a quick and rough estimate about the quality of the recording sites.

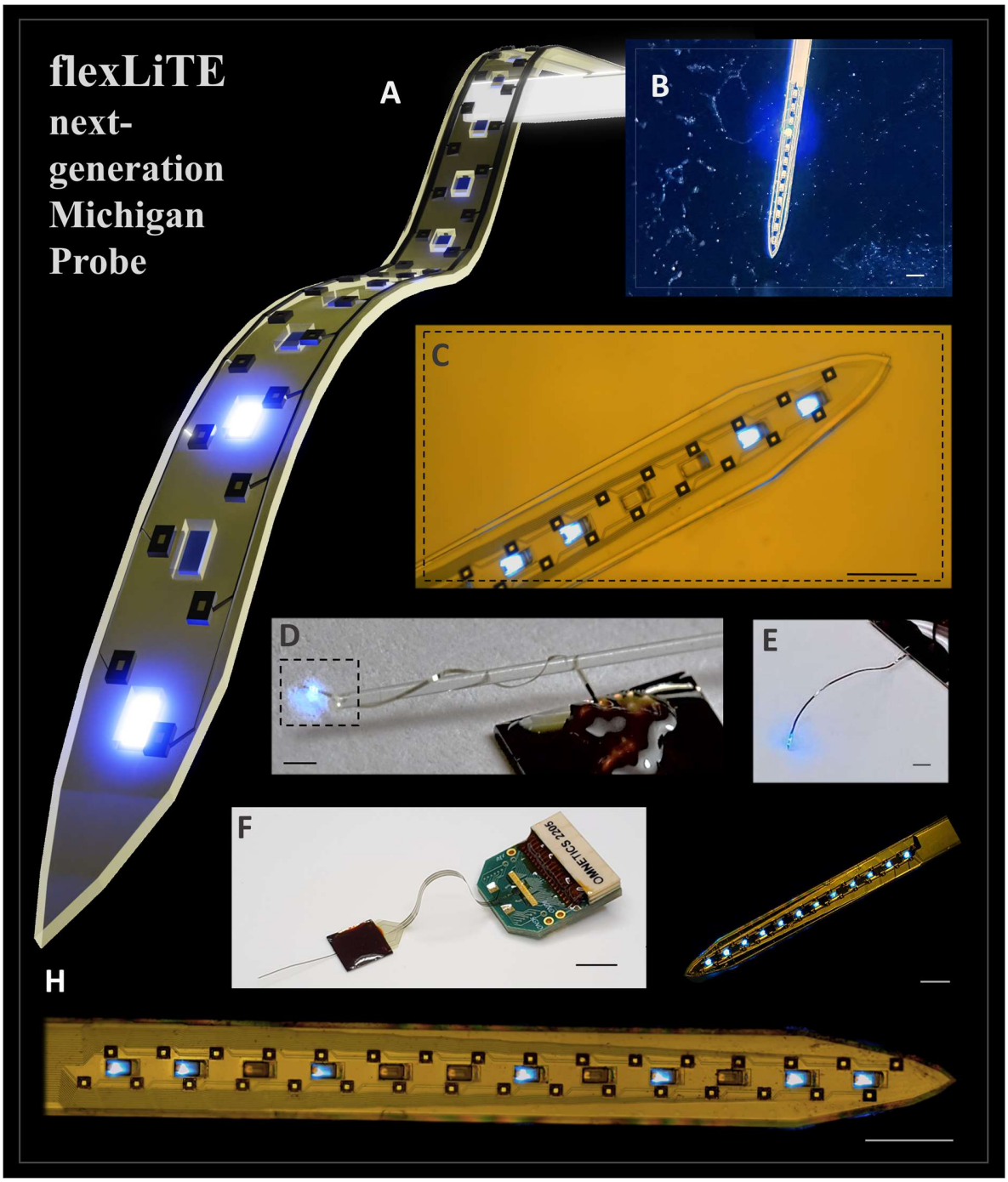

Fig. 1 FlexLiTE optoelectrodes for chronic in-vivo experiments.
A) Schematic image of a flexLiTE optoelectrode with 12 LEDs in a single shank with 32 recording electrodes. Backend of the probe is assembled to an interposer. **B)** Microscope image of a flexLiTE optoelectrode with 12 LEDs in a single shank and 32-recording electrode probe stacked onto the LED probe. Scale bar: 100 µm. **C)** Magnified image of the front end of a flexLiTE optoelectrode. Scale bar: 100 µm **D)** A 10 mm-long shank of the flexLiTE wrapping around a 200

μm diameter optical fiber twice with LEDs turned on. Scale bar: 1 mm. **E)** Bird's eye view of an assembled flexLiTE optoelectrode with LEDs operating. Scale bar: 1 mm. **F)** Fully assembled flexLiTE optoelectrode. The backend of the stacked LED and recording electrode probes are ball bonded to an interposer, and a custom-made cable is connected from the backend of the interposer to a headstage printed circuit board (PCB). Scale bar: 5 mm. **G)** Magnified flexLiTE optoelectrode image with all 12 μILEDs turned on. Scale bar: 100 μm. **H)** Microscope image of the magnified full-view of a flexLiTE optoelectrode with individual μILEDs selectively turned on.

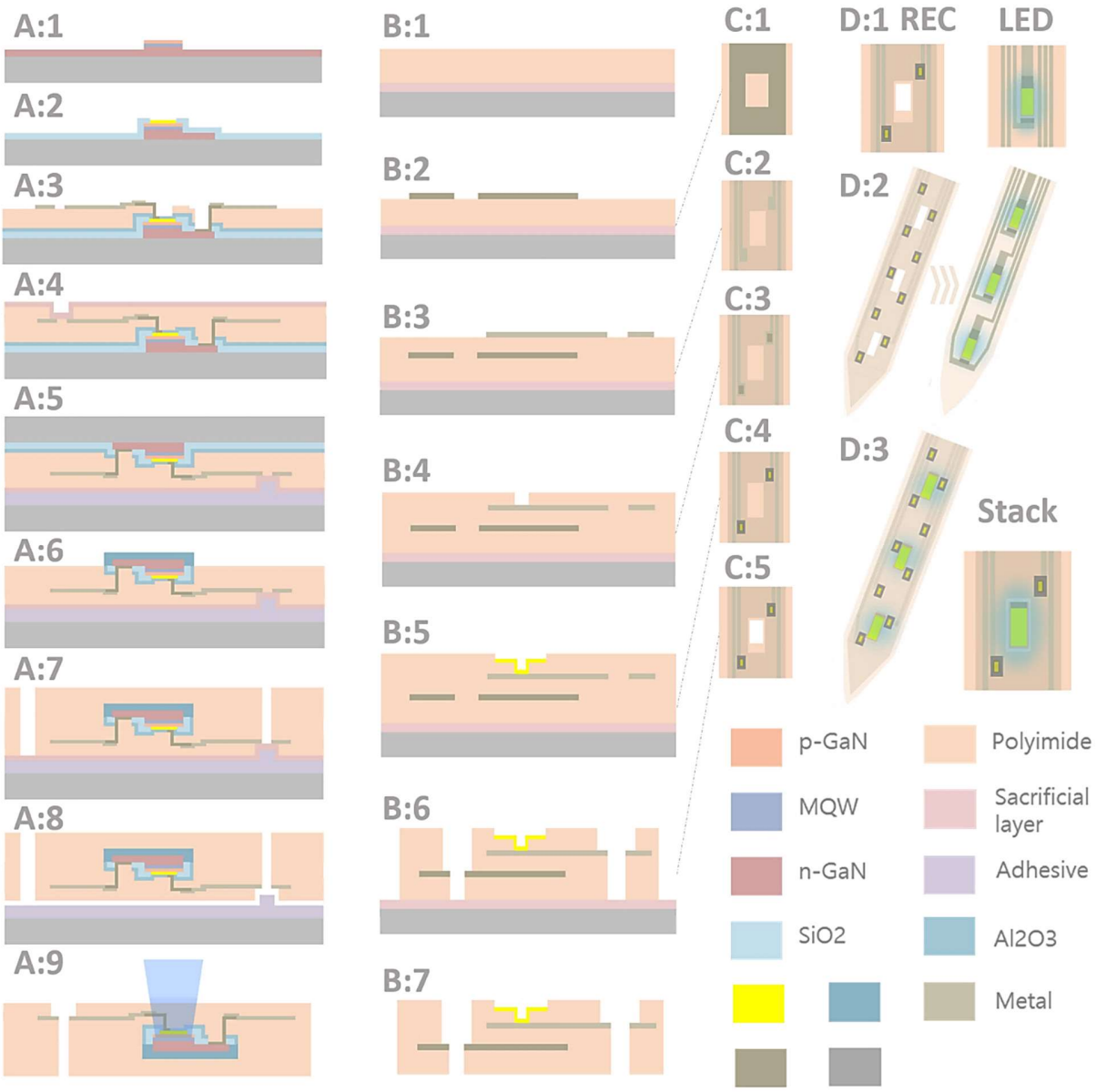

Fig. 2 Fabrication and modular integration of flexLiTE optoelectrodes**.**
A) LED probe fabrication processes. **A-1)** Mesa etching of a GaN-on-silicon wafer to define neuron-size μILEDs. **A-2)** Removal of n-GaN, oxide passivation and p-GaN contact metal definition. **A-3)** Additional oxide passivation, first polyimide layer definition, contact site opening, and metal/trace definition. **A-4)** second polyimide definition, bonding pad opening, and sacrificial layer deposition. **A-5)** Bonding to a transfer wafer through thermal/pressure bonding. **A-6)** Backside substrate removal, oxide removal, LED backside reflector metal definition. **A-7)** third polyimide definition and backside through-hole patterning for ball bonding pad openings. **A-8)** Device release by sacrificial layer removal. **A-9)** Released flexLiTE optoelectrode ready for assembly. **B-C)** Recording electrode probe fabrication process, side view **B)** and top view **C)**. **B-1)** First polyimide layer definition on top of a wafer with sacrificial metal defined. **B-2)** Metal shield defined, excluding the LED window areas. **B-3)** Second polyimide and metal traces for recording sites. **B-4)** Third polyimide layer and electrode-to-trace opening definition. **B-5)** Recording

electrode definition. **B-6)** Bonding pad opening and probe outline definition. **B-7)** Device release for assembly. **C:1-5** corresponding to the top-views of the process steps in B:2-6. Top-view of probe stacking procedures. The LED probe is aligned to the REC probe to place the LEDs inside the LED windows defined in the REC probe. **D:1)** Top-view of the released REC and LED probes. **D:2)** Stacking of the REC probe on top of the LED probe. **D:3)** Stacked top-view of a self-assembled flexLiTE optoelectrode in an aqueous solution.

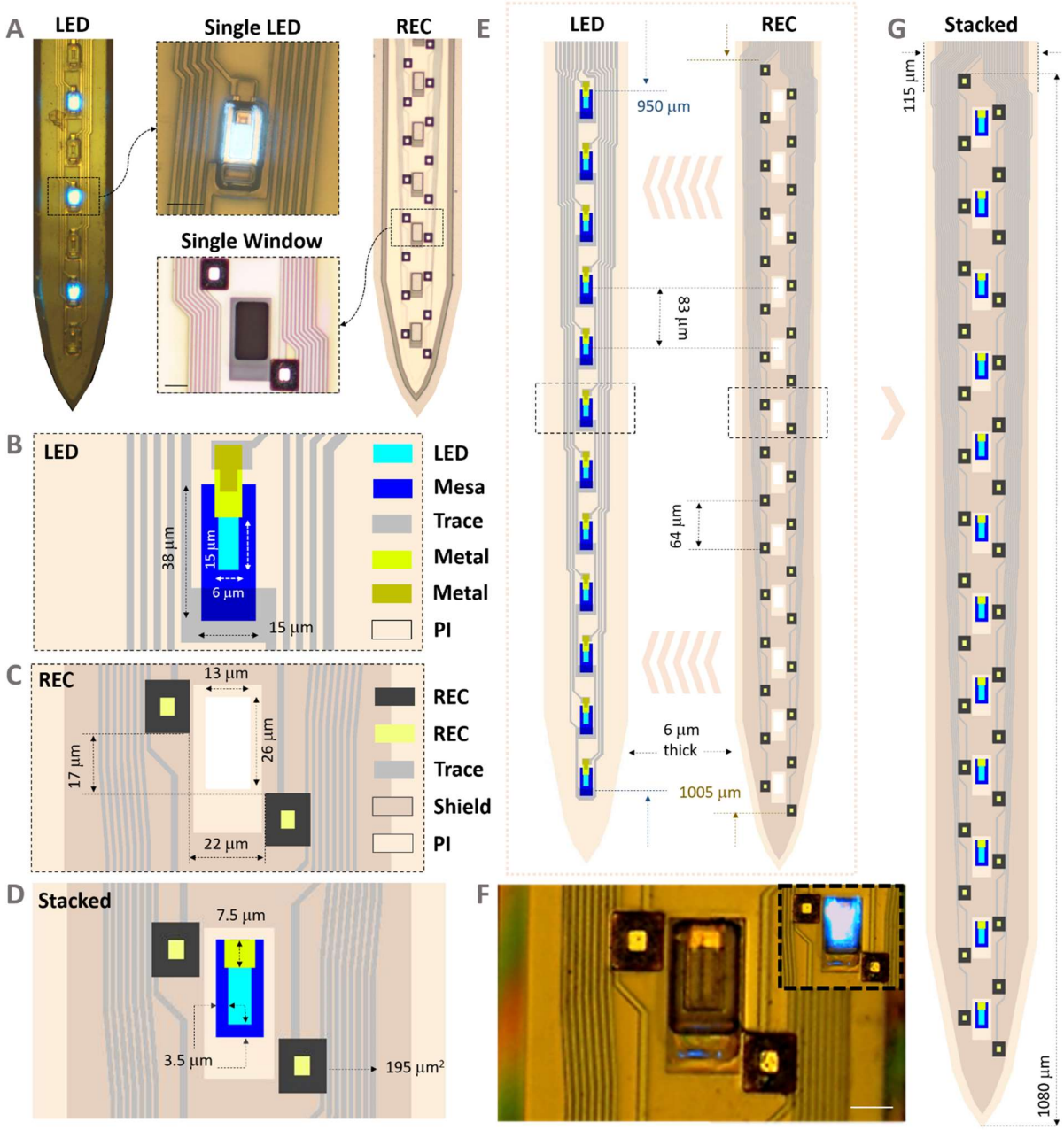

Fig. 3 Modular stacking and assembly of flexLiTE optoelectrodes and critical dimensions. A) Microscope image of the released LED probe (left) and REC probe (right), with enlarge images (center) showing a single LED (top) and a single LED window and two recording electrodes (bottom) (Scale bar: 10 µm). **B)** Schematic of LEDs and dimensions. **C)** Schematic of an LED window and two recording electrodes and dimensions. **D)** Schematic of the stacked probe with an LED aligned to the window of the REC probe. **E)** Schematic of LED and REC probes with design parameters. The REC probe is stacked on top of the LED probe. **F)** Microscope image of the stacked probe showing a LED aligned inside the window of the REC probe. Inset shows the lighting of the LED. Scale bar: 10 µm. **G)** Schematic of the stacked probe with design parameters.

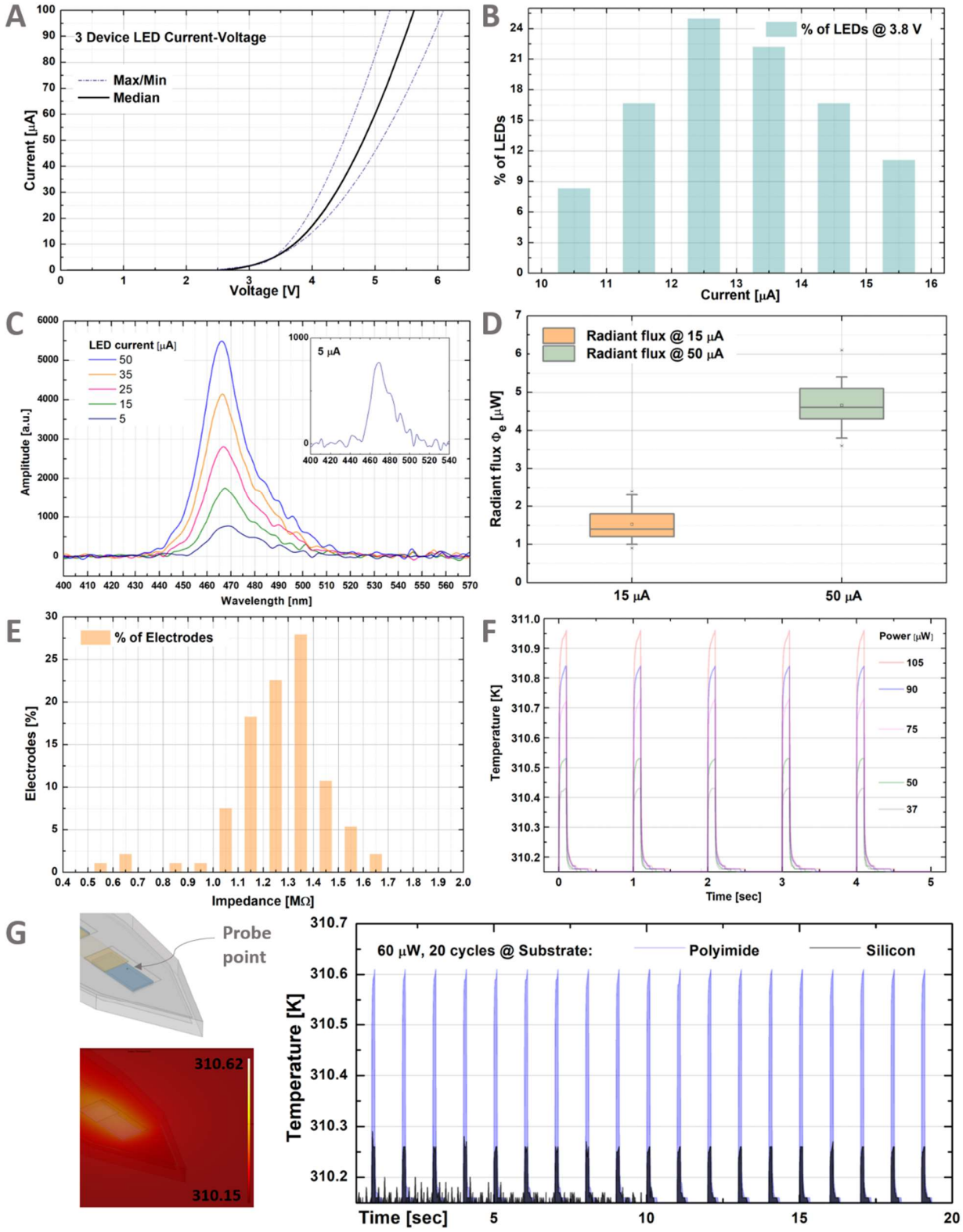
A
3 Device LED Current-Voltage
Max/Min
Median
Current [μA]
Voltage [V]
B
% of LEDs @ 3.8 V
% of LEDs
Current [μA]
C
LED current [μA]
50
35
25
15
5
5 μA
Amplitude [a.u.]
Wavelength [nm]
D
Radiant flux @ 15 μA
Radiant flux @ 50 μA
Radiant flux Φe [μW]
15 μA
50 μA
E
% of Electrodes
Electrodes [%]
Impedance [MΩ]
F
Power [μW]
105
90
75
50
37
Temperature [K]
Time [sec]
G
Probe point
310.62
310.15
60 μW, 20 cycles @ Substrate:
Polyimide
Silicon
Temperature [K]
Time [sec]

Fig. 4 Characteristics of the fabricated flesLiTE optoelectrodes: Bench top testing from three assembled probes and thermal simulation results.
A) LEDs current-voltage characteristics with a compliance current of 100 μA with the maximum and minimum (purple dashed line) and median (black). **B)** Distribution of LED currents at 3.8 V input voltage. **C)** LED light spectra from 5 μA to 50 μA. **D)** Radiant flux box plot for 15 and 50 μA of current. **E)** Impedance distribution of the recording electrodes measured by Intan system. **F)** FEA Thermal simulation results of brain tissue heating for varied power input from 37 μW to 105 μW. Input pulse was set to the exact same square wave that was used during in-vivo testing when driving the LEDs, which is a 10 % duty cycled 1 sec long square pulse. The temperature increase was estimated in the brain tissue 8 um above the surface of an LED. **G)** Comparison of temperature increase between polyimide optoelectrodes and silicon-shank optoelectrodes at 60 μW input power for 20 cycles.

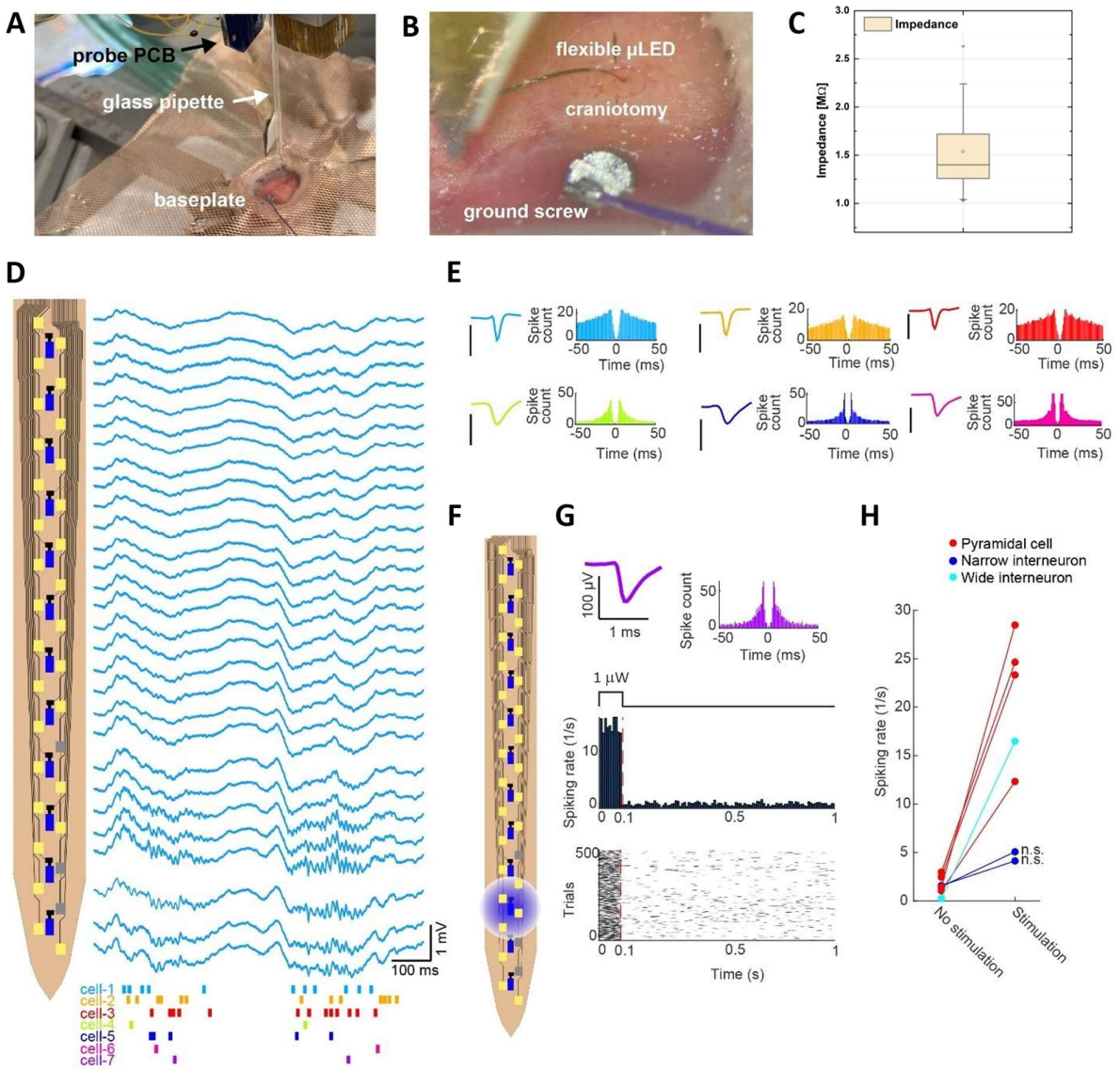

Fig. 5 In vivo opto-electrophysiology with flexLiTE optoelectrodes in freely moving mice.

A-B) Implantation of flexLiTE optoelectrodes. **A)** A flexLiTE optoelectrode is attached to a glass pipette using polyethylene glycol. **B)** After insertion, the glass pipette is retracted leaving behind the flexiLiTE. **C)** Box plot for the impedance of flexLiTE optoelectrodes before surgery. **D)** Left: schematic of the flexLiTE configuration. Blue rectangles show the location of 12 µILEDs and yellow rectangles show the recording sites (grey rectangles are not functioning channels). Right: traces of the recorded wide-band signals (0.1-7500 Hz) and the raster plots of sorted spikes (bottom). **E)** The spiking data was quantified for 7 well-isolated cells (4 putative pyramidal and 3 putative narrow waveform interneurons) recorded simultaneously from CA1 (same color coding as in A). Mean waveform and autocorrelation histogram are shown for each putative single unit (black bar represents 100 µV). **F)** Schematic shows the location of illuminated LED (third LED from the tip of the electrode was used, 1 µW, 467 nm, 100 ms light pulse). **G)** µLED illumination induced spiking around the LED. Plots in the top show mean spike waveforms and autocorrelation

histogram. The putative pyramidal cell was strongly excited by the μLED stimulation, as shown by peristimulus time histogram (middle panel) and raster plot (bottom panel). **H)** Optical modulation of single units (mean firing rate is shown for each putative single unit). Firing rate of 4 pyramidal cells (red circle) and one wide interneuron were modulated by μLED light pulses (2 narrow interneurons were not modulated, n.s. denotes not significant).

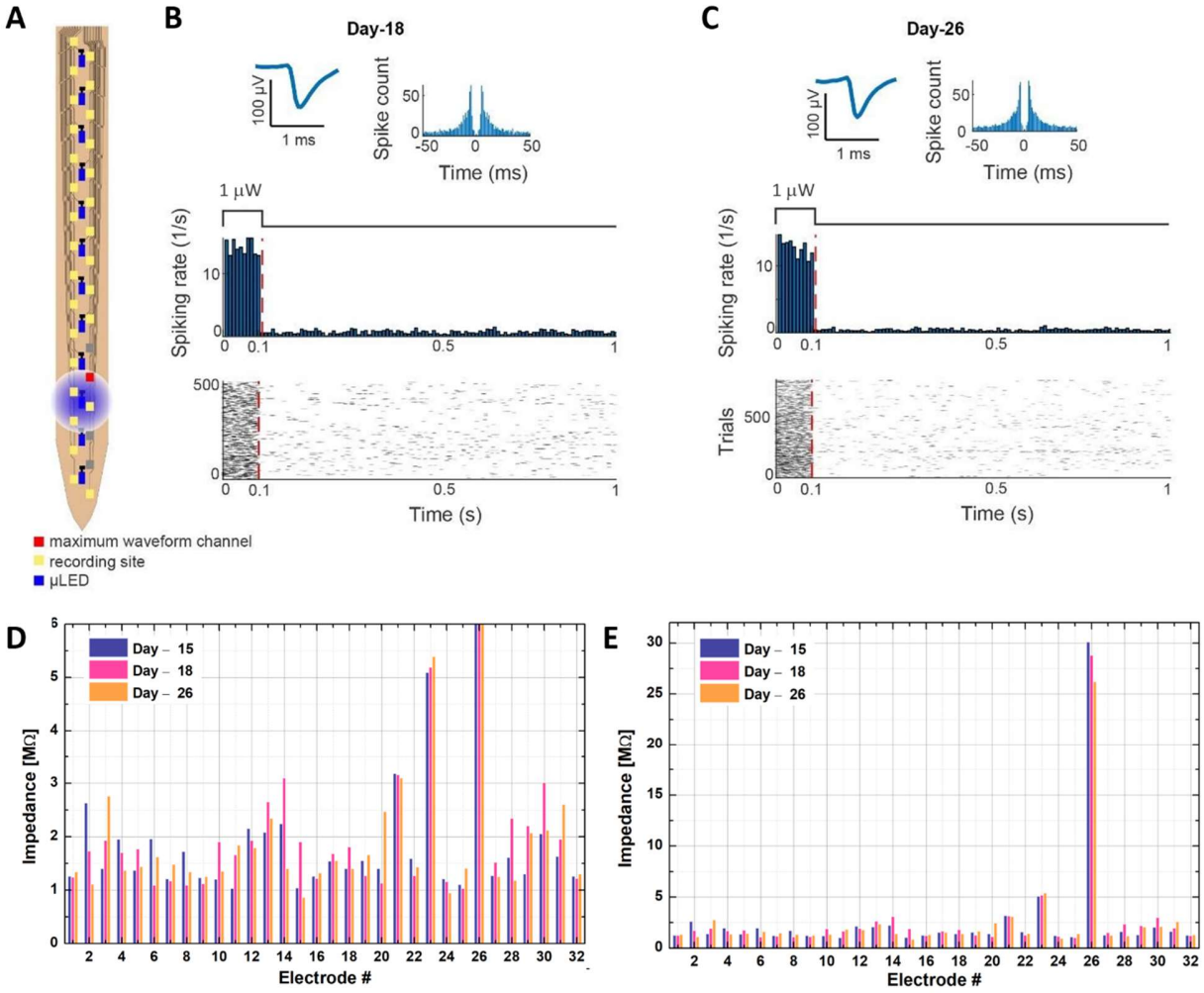

Fig. 6 Readout of input patterns from upstream population activity

A) Schematic of flexLiTE optoelectrodes. Red rectangle shows the location of the maximum waveform amplitude of neurons in B and C. B and C µLED illumination (third LED from the tip of the probe was used, 100 ms, 1 µW, 467 nm) induced spiking on day-18 **B)** and day-26 **C)**. Plots in the top show mean spike waveforms and autocorrelation histogram. The putative pyramidal cells were strongly excited by the µLED stimulation, as shown by peristimulus time histograms (middle panel) and raster plots (bottom panel). **D-E)** Impedance of recording sites measured in-vivo. The impedance of the recording sites was measured using an RHD USB Eval board during each recording session. Left panel shows the channels with the impedance range < 5 MΩ **D)**, and the right panel shows the whole range **E)**.

References

[1] R. Yuste, From the neuron doctrine to neural networks, Nat. Rev. Neurosci. 16, 487-497 (2015).

[2] K. D. Wise, A. M. Sodagar, Y. Yao, M. N. Gulari, E. Perlin, K. Najafi, Microelectrodes, microelectronics, and implantable neural microsystems. Proceedings of the IEEE. 96, 1184-1202, (2008).

[3] M. HajjHassan, V. Chodavarapu, S. Musallam, NeuroMEMS: Neural Probe Microtechnologies. Sensors. 8, 6704-6726, (2008).

[4] J. A. Frank, M.-J. Antonini, P. Anikeeva, Next-generation interfaces for studying neural function. Nature Biotechnology. 37, 1013-1023, (2019).

[5] J. P. Seymour, D. R. Kipke, Neural probe design for reduced tissue encapsulation in CNS. Biomaterials. 28, 3594-3607, (2007).

[6] F. Lotti, F. Ranieri, G. Vadala, L. Zollo, G. D. Pino, Invasive intraneural interfaces: foreign body reaction issues, Front. Neurosci., 11, 497 (2017).

[7] J. E. Chung, H. R. Joo, J. L. Fan, D. F. Liu, A. H. Barnett, S. Chen, C. G.-Breiner, M. P. Karlsson, M. Karlsson, K. Y. Lee, H. Liang, J. F. Magland, J. A. Pebbles, A. C. Tooker, L. F. Greengards, V. M. Tolosa, L. M. Frank, High-density, long-lasting, and multi-region electrophysiological recordings using polymer electrode arrays. Neuron. 101, 21-31, (2019).

[8] H. S. Sohal, G. J. Clowry, A. Jackson, A. O'Neill, S. N. Baker, Mechanical flexibility reduces the foreign body response to long-term implanted microelectrodes in rabbit cortex. Plos One. 11, 10 (2016).

[9] G. Shin, Studies of Parylene/Silicone-coated soft bio-implantable optoelectronic device. Coatings. 10, 404, (2020).

[10] H.-S. Noh, K.-S. Moon, A. Cannon, P. J. Hesketh, C. P. Wong, Wafer bonding using microwave heating of parylene intermediate layers. J. Micromech. Microeng. 14, 625-631, (2004).

[11] L. Luan, X. Wei, Z. Zhao, J. J. Siegel, O. Potnis, C. A. Tuppen, S. Lin, S. Kazmi, R. A. Fowler, S. Holloway, R. A. Chitwood, C. Xie, Ultraflexible nanoelectronic probes form reliable, glial scar-free neural integration. Science Advances. 3, e1601966, (2017).

[12] D. C. Rodger, A. J. Fong, W. Li, H. Ameri, A. K. Ahuja, C. Gutierrez, I. Lavrov, H. Zhong, P. R. Menon, E. Meng, J. W. Burdick, R. R. Roy, V. R. Edgerton, J. D. Weiland, M. S. Humayun, Y.-C. Tai, Flexible parylene-based multielectrode array technology for high-density stimulation and recording. Sensors and Actuators B. 132, 449-460, (2008).

[13] J. W. Reddy, I. Klimulkin, L. T. Stewart, Z. Ahmed, A. L. Barth, E. Towe, M. Chamanzar, High density, double-sided, flexible optoelectronic neural probes with embedded μLEDs, Frontiers in Neuroscience, 13, 745, (2019).

[14] X. Wen, B. Wang, S. Huang, T. L. Liu, M.-S. Lee, P.-S. Chung, Y. T. Chow, I-W. Huang, H. G. Monbouquette, N. T. Maidment, P.-Y. Chiou, Flexible, multifunctional neural probe with liquid metal enabled, ultra-large tunable stiffness for deep-brain chemical sensing and agent delivery. Biosensors and Bioelectronics, 131, 37-45, (2019).

[15] B. Rubehn, T. Stieglitz, In vitro evaluation of the long-term stability of polyimide as a material for neural implants. Biomaterials. 31, 3449-3458, (2010).

[16] M. Vomero, F. Ciarpella, E. Zucchini, M. Kirsch, L. Fadiga, T. Stieglitz, M.

Asplund, On the longevity of flexible neural interfaces: Establishing biostability of polyimide-based intracortical implants. Biomaterials. 281, 121372, (2022).

[17] A. Mercanzini, K. cheung, D. Buhl, M. Boers, A. Maillard, P. Colin, J.-C. Bensadoun, A. Bertsch, A. Carleton, P. Renaud, Demonstration of cortical recording and reduced inflammatory response using flexible polymer neural probes. 2007 IEEE International Conference on MEMS. 573-676.

[18] S. Takeuchi, T. Suzuki, K. Mabuchi, H. Fujita, 3D flexible multichannel neural probe array. J. Micromech. Microeng. 14, 104-107, (2004).

[19] A. Tooker, T. E. Madsen, A. Crowell, K. G. Shah, S. Felix, H. S. Mayberg, S. Pannu, D. G. Rainnie, V. Tolosa, Chronic, multi-contact, neural interface for deep brain stimulation. 2013 6th International IEEE/EMBS Conference on Neural Engineering. 14001630, (2013).

[20] Z. Guo, B. Ji, M. Wang, C. Ge, L. Wang, X. Gu, B. Yang, X. Wang, C. Li, J. Liu, A polyimide-based flexible optoelectrodes for low-noise neural recording. IEEE Electron Device Letters. 40, 1190-1193, (2019).

[21] PI-2600 series product bulletin, HD Microsystems (2009).

[22] S.-Y. Park, K. Na, M. Voroslakos, H. Song, N. Slager, S. Oh, J. P. Seymour, G. Buzsaki, E. Yoon, A miniaturized 256-channel neural recording interface with area-efficient hybrid integration of flexible probes and CMOS integrated circuits. IEEE Trans. Biomed. Eng. 69, 334-346, (2022).

[23] E. Musk, An integrated brain-machine interface platform with thousands of channels, Journal of Medical Internet Research, 21, e16194, (2019).

[24] G. Buzsaki, E. Stark, A. Berenyi, D. Khodagholy, D. R. Kipke, E. Yoon, K. D. Wise, Tools for probing local circuits: high-density silicon probes combined with optogenetics. Neuron. 86, 92-105, (2015).

[25] K. Deisseroth, Optogenetics. Nat Methods. 8, 26-29 (2011).

[26] A. Adamantidis, S. Arber, J. S. Bains, E. Bamberg, A. Bonci, G. Buzsaki, J. A. Cardin, R. M. Costa, Y. Dan, Y. Goda, A. M. Graybiel, M. Hausser, P. Hegemann, J. R. Huguenard, T. R. Insel, P. H. Janak, D. Johnston, S. A. Josselyn, C. Koch, A. C> Kreitzer, C. Luscher, R. C. Malenka, G. Miesenbock, G. Nagel, B. Roska, M. J. Schnitzer, K. V. Shenoy, I. Soltesz, S. M. Sternson, R. W. Tsien, R. Y. Tsien, G. G. Turrigiano, K. M. Tye, R. I. Wilson, Optogenetics:10 years after ChR2 in neurons—views from the community. Nat. Neuro. 18, 1202-1212, (2015).

[27] P. Anikeeva, A. S. Andalman, I. Witten, M. Warden, I. Goshen, L. Grosenick, L. A. Gunaydin, L. M. Frank, K. Deisseroth, Optetrode: a multichannel readout for optogenetic control in freely moving mice. Nat. Neuro. 15, 163-170, (2012).

[28] E. S. Boyden, F. Zhang, E. Bamberg, G. Nagel, K. Deisseroth, Millisecond-timescale, genetically targeted optical control of neural activity. Nat. Neuro. 8, 1263-1268, (2005).

[29] F. Wu, E. Stark, P.-C. Ku, K. D. Wise, G. Buzsaki, E. Yoon, Monolithically integrated μLEDs on silicon neural probes for high-resolution optogenetic studies in behaving animals. Neuron. 88, 1136-1148, (2015).

[30] K. Kampasi, D. F. English, J. Seymour, E. Stark, S. McKenzie, M. Voroslakos, G. Buzsaki, K. D. Wise, E. Yoon, Dual color optogenetic control of neural populations using low-noise, multishank optoelectrodes. Microsystems & Nanoengineering. 4, 10 (2018).

[31] K. Kampasi, E. Stark, J. Seymour, K. Na, H. G. Winful, G. Buzsaki, K. D. Wise,

E. Yoon, Fiberless multicolor neural optoelectrode for in vivo circuit analysis. Sci. Rep. 6, 30961 (2016).

[32] H. Sekiguchi, H. Yasunaga, K. Tsuchiyama, R. Nita, Neural optical probe with monolithically integrated intensity-monitoring μLED and polymer waveguide for optogenetics. Electronic Letters. 55, 619-621 (2019).

[33] Y. Son, H. J. Lee, J. Kim, H. Shin, N. Choi, C. J. Lee, E.-S. Yoon, E. Yoon, K. D. Wise, T. G. Kim, I.-J. Cho, In vivo optical modulation of neural signals using monolithically integrated two-dimensional neural probe arrays. Sci. Rep. 5, 15466 (2015).

[34] A. M. Packer, L. E. Russell, H. W. P. Dalgleish, M. Hausser, Simultaneous all-optical manipulation and recording of neural circuit activity with cellular resolution in vivo. Nature Methods. 12, 140-146, (2015).

[35] K. Kim, M. Voroslakos, J. P. Seymour, K. D. Wise, G. Buzsaki, E. Yoon, Artifact-free and high-temporal-resolution in vivo opto-electrophysiology with microLED optoelectrodes. Nat. Comm. 11, 2063 (22020).

[36] K. Kim, F. Wu, K. D. Wise, E. Yoon, Chapter four – GaN-on-silicon microLEDs for neural interfaces. Semiconductors and Semimetals, Elsevier. 106, 123-172, (2021)

[37] K. Kim, M. Voroslakos, A. F.-Ruiz, S. S. Parizi, E. Ko, B. Hendrix, J. P. Seymour, K. D. Wise, G. Buzsaki, E. Yoon, HectoSTAR microLED optoelectrodes for large-scale, high-precision in vivo opto-electrophysiology. bioRxiv. 2020.10.09.334227.E. Shim, Y. Chen, S. Masmanidis, M. Li, Multisite silicon neural probes with integrated silicon nitride waveguides and gratings for optogenetic applications. BioRxiv. https://doi.org/10.1101/2020.10.09.334227. (2020).

[38] R. Scharf, T. Tsunematsu, N. McAlinden, M. D. Dawson, S. Sakata, K. Mathieson, Depth—specific optogenetic control in vivo with a scalable, high-density μLED neural probe. Sci. Rep. 6, 28381 (2016).

[39] M. Valero, I. Zutshi, E. Yoon, G. Buzsaki, Probing subthreshold dynamics of hippocampal neurons by pulsed optogenetics, Science. 375, 570-574 (2022).

[40] N. Kumar, K. Kennedy, K. Gildersleeve, R. Abelson, C. M. Mastrangelo, D. C. Montgomery, A review of yield modelling techniques for semiconductor manufacturing. International Journal of Production Research. 44, 5019-5036, (2006).

[41] W. Kuo, T. Kim, An overview of manufacturing yield and reliability modeling for semiconductor products. Proceedings of the IEEE. 87, 1329-1344, (1999).

[42] Y.-Q. Yang, Y. Duan, P. Chen, F.-B. Sun, Y.-H. duan, X. Wang, D. Yang, Realization of thin film encapsulation by atomic layer deposition of Al2O3 at low temperature. J. Phys. Chem. C. 117, 20312 (2013).

[43] K. Kim, M. V. Gompel, K. Wu, G. Schiavone, J. Carron, F. Bourgeois, S. P. Lacour, Y. Leterrrier, Extended barrier lifetime of partially cracked organic/inorganic multilayers for compliant implantable electronics. Small. 17, 2103039 (2021).

[44] B. Gysbrechts, L. Wang, N. N. D. Trong, H. Cabral, Z. Navratilova, F. Battaglia, W. Saeys, C. Bartic, Light distribution and thermal effects in the rat brain under optogenetic stimulation. Journal of Biophotonics. 9, 576-585, (2015).

[45] O. Yizhar, L. E. Fenno, T. J. Davidson, M. Mogri, K. Deisseroth, Optogenetics in Neural Systems. Neuron. 71, 9-34, (2011).

[46] M. L. Hufff, R. L. Miller, K. Deisseroth, D. E. Moorman, R. T. LaLumiere, Posttraining optogenetic manipulations of basolateral amygdala activity modulate consolidation of inhibitory avoidance memory in rats. PNAS. 9, 3597-3602, (2013).

[47] B. Mimoun, H. T. M. Pham, V. Henneken, R. Dekker, Residue-free plasma etching of polyimide coatings for small pitch vias with iimproved step coverage. Journal of Vacuum Science &Technology B. 31, 021201, (2013).

[48] C.-A. Cheng, Y.-H. Huang, C.-H. Lin, C.-L. Lee, S.-C. Yang, K.-N. Chen, Wafer-level MOSFET with submicron photolysis polymer temporary bonding technology using ultra-fast laser ablation for 3DIC application. 2016 International Symposium on VLSI-TSA. 1-2, (2016).

[49] T. Itabashi, M. Kotani, M. P. Zussman, K. Zoschke, T. Fischer, M. Topper, H. Ishida, High temperature bonding solutions enabling thin wafer process and handling on 3D-IC manufacturing. 2011 IEEE International 3DIC. 1-4, (2012).

[50] T.-Y. Tsai, C.-H. Lin, C.-L. Lee, S.-C. Yang, K.-N. Chen, An ultra-fast temporary bonding and release process based on thin photolysis polymer in 3D integration. 2015 International 3DIC, TS8.8.1-TS8.8.5, (2015).

[51] H. H. Pennes, Analysis of Tissue and arterial blood temperatures in the resting human forearm, Journal of Appl. Physiol., 1, 93-122, (1948).

[52] M. Voroslakos, H. Miyawaki, S. Royer, K. Diba, E. Yoon, P. C. Petersen, G. Buzsaki, 3D-printed recoverable microdrive and base plate system for rodent electrophysiology. Bio-protocol. 11, e4137, (2021)

[53] M. Pachitariu, N. Steinmetz, S. Kadir, M. Carandini, H. D. Harris, Kilosort: realtime spike-sorting for extracellular electrophysiology with hundreds of channels. BioRxiv, https://doi.org/10.1101/061481. (2016)

[54] P. C. Petersen, J. H. Siegle, N. A. Steinmetz, S. Mahallati, G. Buzsaki, CellExplorer: A framework for visualizing and characterizing single neurons. Neuron. 109, 3594-3608.e2, (2021)

Author contributions

E.K. designed, fabricated (including micro-nanofabrication and assembly), and characterized the flexLiTE optoelectrodes and wrote the manuscript. M.V. performed the in-vivo experiments and analyzed/prepared the in-vivo data and figures. G.B. and E.Y. supervised the project.